

CMTC-486411-MS

Analytical Corrections to CO₂-Brine Core Relative Permeability for Low Rate Flow Modeling

Avinoam Rabinovich, Tel Aviv University

Copyright 2017, Carbon Management Technology Conference

This paper was prepared for presentation at the Carbon Management Technology Conference held in Houston, Texas, USA, 17-20 July 2017.

This paper was selected for presentation by a CMTC program committee following review of information contained in an abstract submitted by the author(s). Contents of the paper have not been reviewed and are subject to correction by the author(s). The material does not necessarily reflect any position of the Carbon Management Technology Conference, its officers, or members. Electronic reproduction, distribution, or storage of any part of this paper without the written consent of the Carbon Management Technology Conference is prohibited. Permission to reproduce in print is restricted to an abstract of not more than 300 words; illustrations may not be copied. The abstract must contain conspicuous acknowledgment of CMTC copyright.

Abstract

Relative permeability of CO₂ and brine is one of the fundamental parameters controlling flow related to carbon storage in saline aquifers. Core samples recovered from subsurface formations are characterized in laboratory experiments to determine effective core relative permeability curves. Typically, coreflooding experiments are conducted at high injection rates so that the resulting flow is viscous dominated. However, at lower rates, it has been shown that the effective curves may change as capillary heterogeneity effects become significant. Using relative permeability determined by conventional coreflooding in simulations with low flow rates, e.g., to model CO₂ migration in aquifers, may incur significant error.

A new method for calculating low flow rate relative permeability curves is presented. The method is based on approximate analytical solutions for effective relative permeability under steady state and capillary limit flow conditions. Derivation is carried out using power law averaging, assuming log normally distributed core permeability. We validate the analytical solution by comparison to numerical solutions for a wide range of cases. An additional correction for the CO₂ curves is shown to be necessary and derived by matching analytical and numerical results. Given a core which has been characterized by conventional high rate coreflooding experiments, the current method gives a fast and efficient correction for low flow rate applications. It circumvents the need for additional experiments or computationally expensive coreflooding simulations.

Introduction

Prediction of CO₂ flow behavior in aquifers is essential for successful large scale storage operations. Numerical modeling is the main tool for conducting such predictions and investigations. A first step in flow modeling is to characterize the properties of the storage reservoir, particularly estimation of the relative permeability, k_{rj} , where j designates phase (CO₂/brine). A common method for obtaining k_{rj} estimations is by CO₂ coreflooding experiments. High injection rates are often used in these experiments to minimize capillary end effects and the resulting curves are therefore limited to high flow rate (viscous dominated) simulations, e.g., flow in regions near CO₂ injection wells. However, accurate modeling of the CO₂ plume migration requires considering the gravity-capillary dominated flow far from the wells (or after wells have been shut off, i.e., post-injection), where flow rates are low. In this case, using the conventional k_{rj} curves may lead to errors in prediction. The goal of this work is to derive analytical formulas which correct the conventional, high flow rate k_{rj} measurements for use in low rate, post-injection CO₂ storage modeling.

Aquifer properties are characterized on various scales. Simulations are conducted on reservoir models of dimension on the order of 100 m to 1 km. These are discretized into grid blocks of typical size 1-10 m while relative permeability is measured on rock samples of smaller, core-scale resolution (order of 10 cm). The measurements are upscaled and assigned to grid blocks for simulation. It is common practice to assign a single set of relative permeability curves to the core sample and to assume that the core is homogeneous, ignoring any sub-core heterogeneity. However, a number of investigations have focused on the small scale, sub-core permeability variations and show that these can affect the large scale flow (Ringrose et al., 1993; Perrin and Benson, 2010; Kuo et al., 2010; Kuo and Benson, 2015; Li and Benson, 2015). The sub-core scale is considered here to be the smallest scale in which Darcy's law still holds (order of 1 mm). In this work, we distinguish between sub-core scale relative permeability curves, k_{rj} , which are considered to be intrinsic properties (we refer to these as characteristic curves), and the core effective (or equivalent) relative permeability k_{rj}^{eff} .

An important feature of sub-core heterogeneity is spatial variations in capillary pressure curves known as capillary heterogeneity. These have been measured directly by Pini et al., 2012 and Pini and Benson (2013). Capillary heterogeneity is often related to the heterogeneities in porosity and permeability, as suggested by the well-known Leverett J-function scaling relationship (Leverett, 1941). Flow at sufficiently low rates is driven by large capillary forces compared to viscous ones and phenomenon such as capillary trapping occurs. In this regime, capillary heterogeneity will also impact coreflooding measurements of k_{rj}^{eff} and these will differ from the characteristic curves (k_{rj}). As a result, k_{rj}^{eff} curves are in fact rate dependent. This has been the focus of attention recently and investigated on the core scale by Perrin et al. (2009); Kuo et al. (2010); Krause (2012a); Kuo and Benson (2015); Krause and Benson (2015) and on larger scales by Virnovsky et al. (2004); Lohne et al. (2006); Neuweiler et al. (2011); Rabinovich et al. (2015).

Evidence has shown that a slight inaccuracy in characterizing the multiphase flow properties can accumulate and lead to significant error in modeling long-term CO₂ sequestration (Li

and Benson, 2015). Particularly, using relative permeability curves which do not incorporate the impact of capillary heterogeneity may incur error in CO₂ storage simulations (Rabinovich et al., 2015). It is therefore paramount to accurately characterize core relative permeability. Coreflooding experiments conducted to estimate relative permeability are based on the extended Darcy's law using measurements of overall pressure drop in the core. Results represent core effective properties (k_{rj}^{eff}) and incorporate capillary heterogeneity effects when these are significant. Therefore, it should be possible to use a single set of k_{rj}^{eff} curves for a given flow rate to characterize the core, thus avoiding sub-core resolution flow modeling. This is demonstrated in Li et al. (2013) Fig. 10 and the discussion therein.

Currently, coreflooding experiments are typically conducted at high flow rates. This is to minimize the capillary end effect, a phenomenon in which the wetting-phase saturation at the core outlet increases due to the abrupt change of capillary pressure (P_c) to zero when phases exit the core (Richardson et al., 1952). Therefore, coreflooding experiments usually measure k_{rj}^{eff} associated with a viscous dominated flow which is equivalent to the characteristic curves, i.e., $k_{rj}^{\text{eff}} = k_{rj}$ is the conventionally used core relative permeability.

For accurate estimation of k_{rj}^{eff} , rate dependent curves departing from k_{rj} should be considered. Ideally, this would entail conducting multiple coreflooding experiments spanning a wide range of injection rates. However, this approach is not likely to be adopted due to the cost and complexity of carrying out many experiments for each core sample. We note that if the core has sufficiently low heterogeneity, k_{rj}^{eff} would not vary significantly and a single set of curves can be used for all flow rates. A more feasible approach is using coreflooding simulations to calculate rate dependent k_{rj}^{eff} (Krause and Benson, 2015). However, this requires estimating an accurate sub-core permeability field which is a difficult problem in itself. Current methods for sub-core permeability estimation (Krause et al., 2013) entail imaging the core with CT scans and applying numerous coreflooding simulations in an iterative process, creating possible cost and complexity issues. It would be very useful to have a simple method to transition from high flow rate k_{rj}^{eff} (equivalent to the characteristic curves) to low flow rate curves for modeling CO₂ migration.

This work presents a semi-analytical approximate solution to core effective relative permeability for capillary dominated flow. It relates between sub-core properties: k_{rj} , P_c , k_G (permeability geometric mean) and σ_y^2 (variance of log-permeability, $y = \ln k$), and core effective properties k_{rj}^{eff} . The solution allows to easily transition from the conventional $k_{rj}^{\text{eff}} = k_{rj}$, measured from viscous dominated (high rate) coreflooding experiments, to new curves which can be used to model low rate CO₂ migration more accurately. The effective property problem is simplified by assuming capillary limit conditions, a reasonable assumption for upscaling CO₂ storage simulations (Mouche et al., 2010; Behzadi and Alvarado, 2012). Log normally distributed permeability (k) is further assumed and an estimation of the core k statistical properties (k_G and σ_y^2) is required. The solution is based on power law averaging and heuristic formulas to correct the CO₂ relative permeability curves. Corrections are shown to be particularly important for cases of P_c curves exhibiting capillary entry pressure. Extensive validation is carried out by comparing the new solution to numerical calculations for a wide range of cases, i.e, varying σ_y^2 , P_c curves and k_{rj} curves.

We note that the current formula considers only drainage coreflooding experiments and deriv-

ing k_{rj}^{eff} for imbibition is not addressed. Furthermore, we consider isotropic k here and anisotropic correlation structures should be considered in the future. This work is an extension to the two-dimensional case of effective relative permeability presented in Rabinovich et al. (2016). The solution is extended here to three-dimensions and also considers additional complications such as capillary entry pressure effects. In fact, the CO₂ relative permeability solution here is found to be quite different from the 2D case due to these effects. Moreover, Rabinovich et al. (2016) do not consider the various aspects of applications to core modeling.

Problem statement

We model coreflooding experiments as immiscible flow of supercritical CO₂ and brine assuming incompressible rock and flowing phases. Similar coreflooding models have been considered by Krause (2012b) and Li (2014). The governing equations are obtained from a mass balance and the extended Darcy's law for each phase. They are given by

$$\phi \frac{\partial S_j}{\partial t} - \nabla \cdot \left[\frac{k_{rj}}{\mu_j} \mathbf{k} \cdot \nabla (p_j + \rho_j g z) \right] = 0, \quad (1)$$

where ϕ is the porosity of the rock, S_j the saturation of phase j ($j = \text{CO}_2$ or $j = w$ for water/brine phase), k_{rj} the relative permeability to phase j , μ_j the viscosity of phase j , \mathbf{k} the absolute permeability tensor, p_j the pressure of phase j , ρ_j is phase density, g is gravitational acceleration, and z is the vertical coordinate. The constraint $S_w + S_{\text{CO}_2} = 1$ applies and the pressures of the nonwetting phase and the wetting phase are related by

$$p_{\text{CO}_2} - p_w = P_c(S_w), \quad (2)$$

where P_c is capillary pressure.

Given the three sub-core properties: \mathbf{k} , $P_c(S_w)$ and $k_{rj}(S_w)$, we seek to find the core effective property k_{rj}^{eff} . Isotropic permeability is assumed so that $k(x, y, z)$ is a scalar function of space, i.e., $k_x = k_y = k_z$ and (x, y, z) is the three-dimensional Cartesian coordinate system, where x is aligned with the direction of flow injection. The $P_c(S_w)$ curve can be obtained using various laboratory measurement techniques (Omorgle, 1988). We adopt the J -function approach (Leverett, 1941) to model capillary heterogeneity; i.e.,

$$P_c(S_w, k) = \alpha \sqrt{\frac{\phi}{k}} J(S_w), \quad (3)$$

where α is a scaling coefficient which accounts for interfacial tension, contact angle and unit conversion. Two of the most widely used J -functions are the Brooks-Corey (Brooks and Corey, 1966) (denoted BC) and van Genuchten (van Genuchten, 1980) (denoted VG) models given by

$$J_{BC}(S_w) = (\tilde{S}_w)^{-1/\lambda} \quad (4)$$

and

$$J_{VG}(S_w) = \left[(\tilde{S}_w)^{-1/m} - 1 \right]^{1-m}, \quad (5)$$

respectively, where λ and m are fitting parameters, $\tilde{S}_w = (S_w - S_{wi})/(1 - S_{wi})$ and S_{wi} is the irreducible wetting phase saturation. We note that these are drainage curves and therefore hysteresis effects are not considered.

Eq. (3) with a single J -function has been used to represent sub-core capillary pressure in numerical and experimental work (e.g., Kuo et al. (2010), Krause et al. (2013) and Wei et al. (2014)). Sometimes, it is further assumed that the global (effective) core capillary pressure has the same structure (Pini et al., 2012; Krause et al., 2013). In this work, only the sub-core scale P_c is assumed to be of the type presented in Eq. (3) with a given J -function. However, in experimental settings, P_c should be measured carefully to insure it is representative of the sub-core scale as it may differ from the core effective P_c curves.

Core characteristic relative permeability k_{rj} are typically measured directly via high flow rate coreflooding experiments. The most widely applied techniques are steady state or unsteady methods. Considering the steady state method, a mixture of the two phases is injected into the fully brine saturated core at a given rate and fractional flow until steady state is reached. The curves are measured using extended Darcy's law as follows

$$k_{rj} = \frac{q_j \mu_j L}{k^{\text{eff}} A \Delta p_j}, \quad (6)$$

where q_j is the injection rate (flux) of phase j , Δp_j is the phase pressure difference between inlet and outlet, L is core length, A is the area perpendicular to flow and k^{eff} is the core effective absolute permeability. Each experiment consisting of a given injection fractional flow produces a point in the k_{rj}^{eff} curves and fractional flows are varied between 100% and 0% to obtain the full curves. The experiment with 100% brine injection results in single phase flow which by Darcy's Law yields the absolute permeability, i.e.,

$$k^{\text{eff}} = \frac{q_w \mu_w L}{A \Delta p_w}. \quad (7)$$

We consider here a common model for uniform drainage characteristic curves given by

$$k_{rw} = (\tilde{S}_w)^{n_w}, \quad (8a)$$

$$k_{r\text{CO}_2} = \kappa_r^{\text{max}} (1 - \tilde{S}_w)^{n_{\text{CO}_2}}, \quad (8b)$$

where κ_r^{max} , n_w and n_{CO_2} are fitting parameters determined by matching Eqs. (8a,b) to experimental results (Eqs. (6) and (7)). We note that for coreflooding measurements to be equivalent to characteristic curves, k_{rj} must be uniform in the core. This is typically assumed for core samples of a given lithofacies and consistent with the assumption of a single J -function in the core.

If total injection rate $q = q_w + q_{\text{CO}_2}$ in the coreflooding experiments described above is not large enough and the core is heterogeneous, the measured relative permeability curves will no longer represent characteristic curves, but rather effective curves $k_{rj}^{\text{eff}} \neq k_{rj}$. At sufficiently low q , when the capillary forces dominate compared to viscosity (capillary limit), k_{rj}^{eff} will converge to a given function of saturation, independent of injection rate. These low injection rate curves are the capillary limit (CL) effective curves and our goal is to derive semi-analytical expressions for these $k_{rj}^{\text{eff}}(S_w)$ curves.

Capillary limit effective relative permeability

The CL method of upscaling is described in the literature (e.g., Pickup and Sorbie (1996), Rabinovich et al. (2016)) and a short summary is presented in the following. We assume steady state, small viscous pressure gradients compared to capillary pressure gradients and negligible impact of gravity. The flowing phases are therefore in capillary equilibrium in which P_c is constant. Thus, for a given constant value of $P_c(\tilde{S}_w, k) = \hat{P}_c$, the saturation field is obtained by inversion as follows

$$\tilde{S}_w(x, y, z) = P_c^{-1}(\hat{P}_c, k(x, y, z)), \quad (9)$$

where constant core porosity ϕ is assumed. The spatial variation of relative permeability is now given by the relationship $k_{rj}(x, y, z) = k_{rj}(\tilde{S}_w)$ with \tilde{S}_w given by Eq. (9). Furthermore, the phase permeability is known and given by

$$K_j(x, y, z) = k_{rj}(\tilde{S}_w) \cdot k(x, y, z) = k_{rj}(P_c^{-1}(\hat{P}_c, k(x, y, z))) \cdot k(x, y, z). \quad (10)$$

If we now relax the CL assumption, allowing flow in the system, but still use the CL relationships, the problem reduces to two separate flow problems

$$\nabla \cdot \left[\frac{K_w(x, y, z)}{\mu_w} \nabla p_w \right] = 0, \quad (11a)$$

$$\nabla \cdot \left[\frac{K_{CO_2}(x, y, z)}{\mu_{CO_2}} \nabla p_{CO_2} \right] = 0, \quad (11b)$$

where $K_j(x, y, z)$ are known functions given by (10). Typical boundary conditions for an effective property problem are considered - given constant pressure at the inlet (p_j^{in}) and outlet (p_j^{out}) of the core and no-flow condition on the curved face of the cylinder. The core effective phase permeability is defined similar to a single phase flow k^{eff} problem as

$$K_j^{eff} = \frac{\langle q_{j,x} \rangle \mu_j L}{A (p_j^{in} - p_j^{out})}, \quad (12)$$

where $\langle q_{j,x} \rangle$ is the average flux of phase j in the direction of flow injection. The core effective relative permeability is then given by

$$k_{rj}^{eff} = \frac{K_j^{eff}}{k^{eff}}. \quad (13)$$

The procedure for CL k_{rj}^{eff} calculation can be summarized as follows:

1. Calculate k^{eff} from a coreflood experiment by Eq. (7).
2. Choose a value \hat{P}_c of capillary pressure.
3. Calculate the saturation field $\tilde{S}_w(k)$ by Eq. (9) and $\langle \tilde{S}_w \rangle$ by arithmetic averaging of \tilde{S}_w .
4. Calculate K_j^{eff} by Eq. (12) for a given realization of k (or by an analytical approach as done in the following), substituting Eq. (10) in Eqs. (11a) and (11b) and solving numerically to obtain $\langle q_{j,x} \rangle$.

5. Obtain the point $\left(\langle \tilde{S}_w \rangle, k_{rj}^{\text{eff}}\right)$, with k_{rj}^{eff} from Eq. (13).
6. Repeat steps 2-5 for different choices of \hat{P}_c , scanning values of $\langle \tilde{S}_w \rangle$ from 0 to 1 to generate the complete k_{rj}^{eff} curves.

Semi-analytical solution

We now derive semi-analytical expressions for k_{rj}^{eff} . The CL method is used as described in the previous section, however, the numerical solution of the equations in step 4 will not be necessary and instead, closed form formulas for K_j^{eff} will be proposed. This will allow carrying out calculations with hardly any computational cost.

Assuming the VG J -function of Eq. (5) in capillary pressure (Eq. (3)) we can invert as described in Eq. (9) to obtain

$$\tilde{S}_w(\tilde{P}_c, k) = \left[\left(\tilde{P}_c \sqrt{k} \right)^{\frac{1}{1-m}} + 1 \right]^{-m}, \quad (14)$$

where $\tilde{P}_c = \hat{P}_c / (\alpha \sqrt{\phi})$ is a constant which will be varied between zero and infinity to cover the full range of saturations ($0 < \langle \tilde{S}_w \rangle < 1$), as noted in step 6 in the previous section. Then, an expression for K_j is derived by substitution of Eq. (14) in Eqs. (8a,b) to arrive at

$$K_w(\tilde{P}_c, k) = k \left[\left(\tilde{P}_c \sqrt{k} \right)^{\frac{1}{1-m}} + 1 \right]^{-n_w m} \quad (15a)$$

$$K_{\text{CO}_2}(\tilde{P}_c, k) = \kappa_r^{\text{max}} k \left\{ 1 - \left[\left(\tilde{P}_c \sqrt{k} \right)^{\frac{1}{1-m}} + 1 \right]^{-m} \right\}^{n_{\text{CO}_2}}. \quad (15b)$$

A similar derivation is carried out for the BC J -function of Eq. (4) to arrive at

$$\tilde{S}_w(\tilde{P}_c, k) = \begin{cases} \tilde{P}_c k^{-\lambda/2}, & \tilde{P}_c k^{-\lambda/2} < 1 \\ 1 & \tilde{P}_c k^{-\lambda/2} > 1 \end{cases}, \quad (16)$$

which then by substitution in Eq. (8a,b) gives

$$K_w(\tilde{P}_c, k) = \begin{cases} \tilde{P}_c^{n_w} k^{1-\lambda n_w/2}, & \tilde{P}_c k^{-\lambda/2} < 1 \\ 1 & \tilde{P}_c k^{-\lambda/2} > 1 \end{cases} \quad (17a)$$

$$K_{\text{CO}_2}(\tilde{P}_c, k) = \begin{cases} \kappa_r^{\text{max}} k \left(1 - \tilde{P}_c k^{-\lambda/2} \right)^{n_{\text{CO}_2}}, & \tilde{P}_c k^{-\lambda/2} < 1 \\ 0 & \tilde{P}_c k^{-\lambda/2} > 1 \end{cases}. \quad (17b)$$

The piecewise functions in Eqs. (16) and (17a,b) are used to ensure that unphysical values of $\tilde{S}_w > 1$ are eliminated. This is an important feature resulting from the inclusion of capillary entry pressure in the BC type $P_c(\tilde{S}_w)$ model, i.e., for $\tilde{S}_w = 1$, P_c is nonzero as seen in Eq. (4). Such K_{CO_2} fields are challenging to average because many methods such as the geometric mean will

(by definition) average to zero if any point in the field is zero, resulting in possibly meaningless averages.

We first consider layered permeability briefly. It is well known that $k^{\text{eff}} = k_A$, the arithmetic mean, for flow parallel to the layers, and $k^{\text{eff}} = k_H$, the harmonic mean, for flow perpendicular to the layers. This result has been extended to CL effective relative permeability by Corey and Rathjens (1956), Virnovsky et al. (2004) and Rabinovich et al. (2016), where an exact solution is given by

$$k_{rj}^{\text{eff}} = \frac{[K_j]_A}{k^{\text{eff}}}, \quad (18)$$

for flow parallel to the layers, and

$$k_{rj}^{\text{eff}} = \frac{[K_j]_H}{k^{\text{eff}}}, \quad (19)$$

for flow perpendicular to the layers, where K_j are given here by Eqs. (15a,b) or (17a,b). Therefore, if core samples exhibit layered permeability, a transition to low flow rate curves is straightforward using Eqs. (18) and (19).

The core can be further modeled as comprised of numerous layers, each with permeability drawn from a distribution of known probability density function (PDF). Eqs. (18) and (19) are then expressed as the following integrals

$$k_{rj}^{\text{eff}} = \frac{1}{k_A} \int_{-\infty}^{\infty} K_j(\tilde{P}_c, k) p(k) dk, \quad (20)$$

$$k_{rj}^{\text{eff}} = \frac{1}{k_H} \left[\int_{-\infty}^{\infty} K_j(\tilde{P}_c, k)^{-1} p(k) dk \right]^{-1}, \quad (21)$$

where $p(k)$ is the PDF of the distribution. The corresponding arithmetic average of \tilde{S}_w is given by

$$\langle \tilde{S}_w \rangle = \int_{-\infty}^{\infty} \tilde{S}_w(\tilde{P}_c, k) p(k) dk. \quad (22)$$

Next, log-normal permeability fields are considered such that $y = \ln k$ is normally distributed and characterized by the mean k_G and variance σ_y^2 . Such fields are commonly considered on a range of scales Freeze (1975), and have been found to apply also to sub-core permeability (see Fig. 9 in Rabinovich (2017)). An isotropic correlation structure is assumed, i.e., $l_x = l_y = l_z$, where l_x , l_y and l_z are the dimensionless correlation lengths in the x , y and z directions (nondimensionalized by the domain length in the corresponding direction). Under these conditions, Rabinovich (2017) found that the approximation

$$k_{rw}^{\text{eff}} = \frac{[K_w]_G \left(1 + \sigma_{\Gamma_w}^2/6 + \sigma_{\Gamma_w}^4/72 \right)}{k^{\text{eff}}} \quad (23)$$

applies to cases of sufficiently small variance of log phase permeability $\sigma_{\Gamma_w}^2$, where $\Gamma_w = \ln K_w$. However, it has been shown in Rabinovich et al. (2016) that for $k_{r\text{CO}_2}^{\text{eff}}$, variance $\sigma_{\Gamma_{\text{CO}_2}}^2$ are much larger and errors for Eq. (23) are generally large. We therefore adopt a different approach, also used in Rabinovich et al. (2016) and Rabinovich (2017), of power law averaging.

Power law averaging is a heuristic method for calculating effective permeability in one-, two- and three-dimensional k fields (Journel et al., 1986; Deutsch, 1989). For a discrete permeability field, e.g., a numerical grid, the averaging is as follows

$$k^{\text{eff}} = \left(\sum_{i=1}^N v_i k_i^\omega \right)^{1/\omega}, \quad (24)$$

where v_i is the volume fraction associated with permeability $k_i = \{k_1, k_2, k_3 \dots k_N\}$ and ω is the power used for averaging. For continuous k the power average is given by

$$k^{\text{eff}} = \left\{ \int_{-\infty}^{\infty} k^\omega p(y) dy \right\}^{1/\omega}, \quad (25)$$

where $p(y)$ is the PDF of $y = \ln k$.

In analogy to Eq. (25) and following Rabinovich et al. (2016); Rabinovich (2017), we propose using power law averaging for the calculation of k_{rj}^{eff} , i.e.,

$$k_{rj}^{\text{eff}} = \frac{1}{k^{\text{eff}}} \left\{ \int_{-\infty}^{\infty} [K_j(\tilde{P}_c, k)]^\omega p(y) dy \right\}^{1/\omega}, \quad (26)$$

where $K_j(\tilde{P}_c, k)$ is given by Eqs. (15a,b) or (17a,b). The value of ω used in Eq. (26) is determined by solving Eq. (25) where k^{eff} is known from coreflooding measurements. Values are between $\omega = -1$ (harmonic average), representing flow perpendicular to layered media, and $\omega = 1$ (arithmetic average), representing flow parallel to layers. For 2D isotropic media ω tends to zero, equivalent to geometric averaging.

The solution for k_{rw}^{eff} obtained by substituting Eqs. (15a,b) or (17a,b) in Eq. (26) is semi-analytical (although we may refer to this solution as analytical) since an integral remains to be solved numerically. A fully analytical solution is achievable by solving the integrals using series expansions (see Rabinovich et al. (2016) Section 5), however performing the numerical quadrature is favorable for many cases, both in simplicity and calculation time, and in the next section, calculations are carried out with the semi-analytical solution. We note that the solution proposed here is an approximate one and the error will be evaluated in the next section, where corrections to the CO_2 curves will also be discussed.

Results

In this section, the approximate semi-analytical solution for the CL effective relative permeability curves k_{rw}^{eff} is tested against numerical calculations. We assume the sub-core characteristic curves have been measured in high flow rate coreflooding experiments and fitted by the function shown in Eqs. (8a,b). A few values of n_w and n_{CO_2} will be considered in these equations. A value of $\kappa_r^{\text{max}} = 0.8$, i.e., the maximum CO_2 relative permeability (obtained at $\tilde{S}_w = 0$), is taken consistently. This parameter is a constant in our formulation and changing its value is not expected to

have a significant impact on the results presented here. We further assume that $P_c(\tilde{S}_w)$ curves have been measured experimentally, e.g., using mercury injection capillary pressure, and the J -function results have been fitted with a VG (Eq. (4)) or BC (Eq. (5)) model. The impact of varying λ and m parameters will be considered.

The numerical solutions are obtained through the following procedure. Three dimensional permeability realizations are generated by sequential Gaussian simulation (Deutsch and Journel, 1992) using the Stanford Geostatistical Modeling Software, SGeMS (Remy et al., 2009). Core samples are taken to be rectangular for simplicity. Then, Eqs. (11a,b), with specified phase pressure boundary conditions, are solved using Stanford's General Purpose Research Simulator, GPRS (Cao, 2002), and K_j^{eff} is calculated via Eq. (12), which gives k_{rj}^{eff} by Eq. (13). In all cases the permeability fields are defined on $50 \times 25 \times 25$ grids. A separate simulation is required to generate each data point on every effective relative permeability curve.

Van Genuchten capillary pressure

Results for VG capillary pressure are considered in this section. In Fig. 1, a comparison between the new analytical k_{rw}^{eff} and numerical calculations is presented for three variances (σ_y^2). Parameters of $m = 0.75$ and $n_w = n_{\text{CO}_2} = 2$ are taken, used in the past for CO₂-brine coreflooding simulations (Bielinski, 2007; Rabinovich et al., 2016). The analytical water curves, given by substituting Eq. (15a) in Eq. (26), are shown to accurately match the numerical ones for all 3 cases. The CO₂ curves (substituting Eq. (15b) in Eq. (26)) show a slight error for larger σ_y^2 , however, a correction, which will be discussed in the following, is used and the corrected curves (dashed lines) are accurate. The values of ω used in Eq. (26) are indicated below the figures and it can be seen they are not sensitive to changes in σ_y^2 .

The characteristic curves are also plotted in Fig. 1 for comparison. It can be seen that as heterogeneity increases (larger σ_y^2), k_{rj}^{eff} curves are more distant from the characteristic curves, which is expected due to the increasing impact of capillary heterogeneity. Furthermore, the CO₂ curves (without correction) show more departure from the numerical curves as σ_y^2 grows. This is also observed in Fig. 2a, where the $k_{r\text{CO}_2}^{\text{eff}}$ error (red line) is plotted as a function of σ_y^2 and seen to be increasing. The error is taken here as the maximum difference between analytical and numerical solutions, i.e., $\max \left| \left(k_{rj}^{\text{eff}}(\langle \tilde{S}_w \rangle) \right)_A - \left(k_{rj}^{\text{eff}}(\langle \tilde{S}_w \rangle) \right)_N \right|$, where A denotes analytical and N denotes numerical. The water curves (blue line), however, do not exhibit a consistent increase in error with σ_y^2 and furthermore the errors are smaller in comparison to the CO₂ curves.

The impact of σ_y^2 on the accuracy of the analytical method and the different behaviour of the water and CO₂ curves was investigated extensively in Rabinovich et al. (2016) for the two-dimensional case with geometric averaging (as opposed to the power law averaging used here). It was shown that larger variance of $\ln K_j$ (denoted $\sigma_{\Gamma_j}^2$) are associated with larger error in the method. This can be explained with effective property theory for geometric averaging in the 2D case, however the same theory does not apply to our case. Nevertheless, we found the behaviour to be similar, as shown in Fig. 2b. Here, it can be seen that increasing σ_y^2 leads to a larger $\langle \sigma_{\Gamma_j}^2 \rangle$ and this in turn is associated with a larger error as seen in Fig. 2a. Average $\sigma_{\Gamma_j}^2$ is taken here because each point on the curve has a different $\sigma_{\Gamma_j}^2$ corresponding to $\langle \tilde{S}_w \rangle$ values.

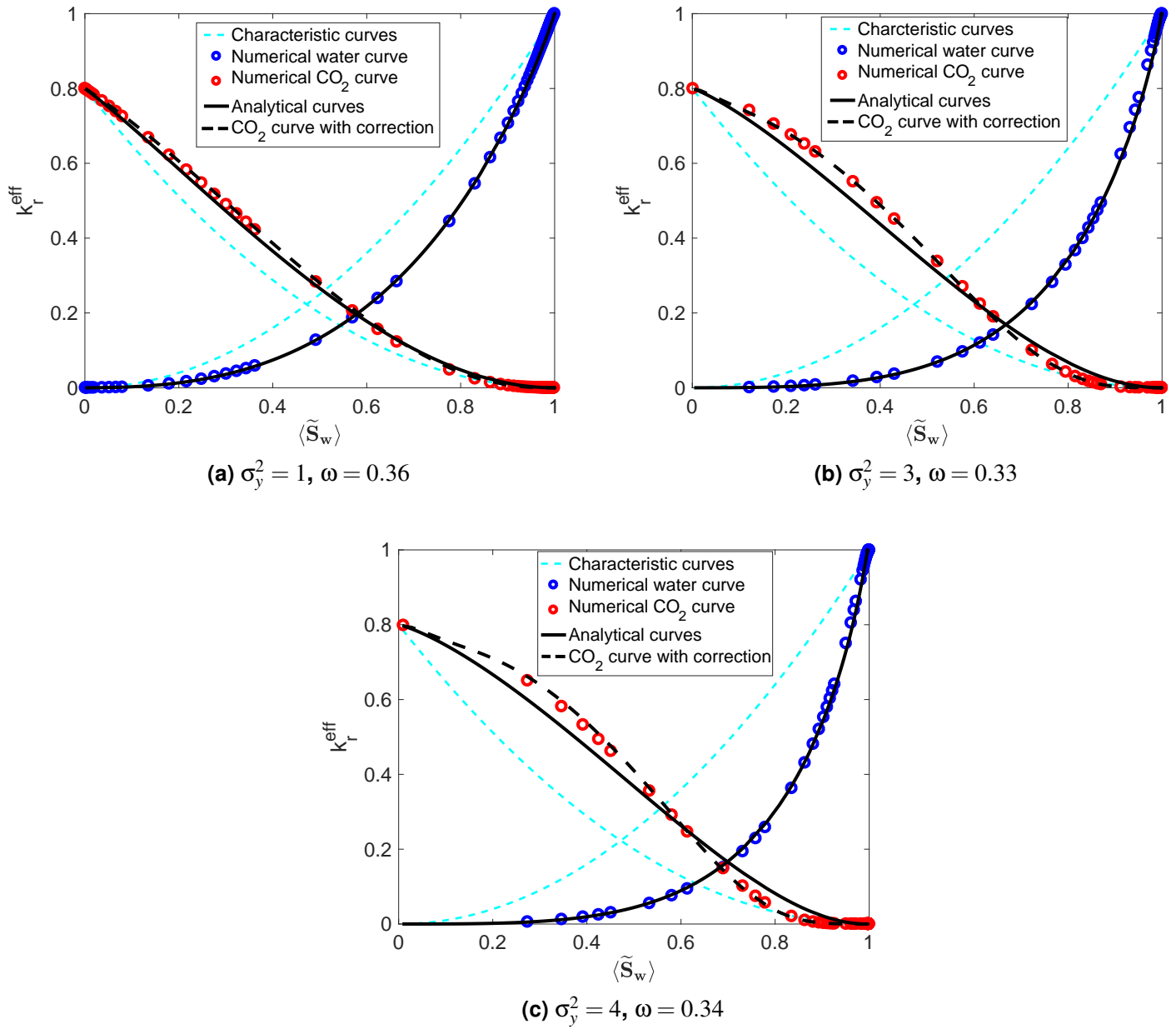


Figure 1: Core effective relative permeability as a function of water saturation in isotropic media with $l_x = l_y = l_z = 0.1$, $k_G = 100$ md, assuming VG J-function with $m = 0.75$.

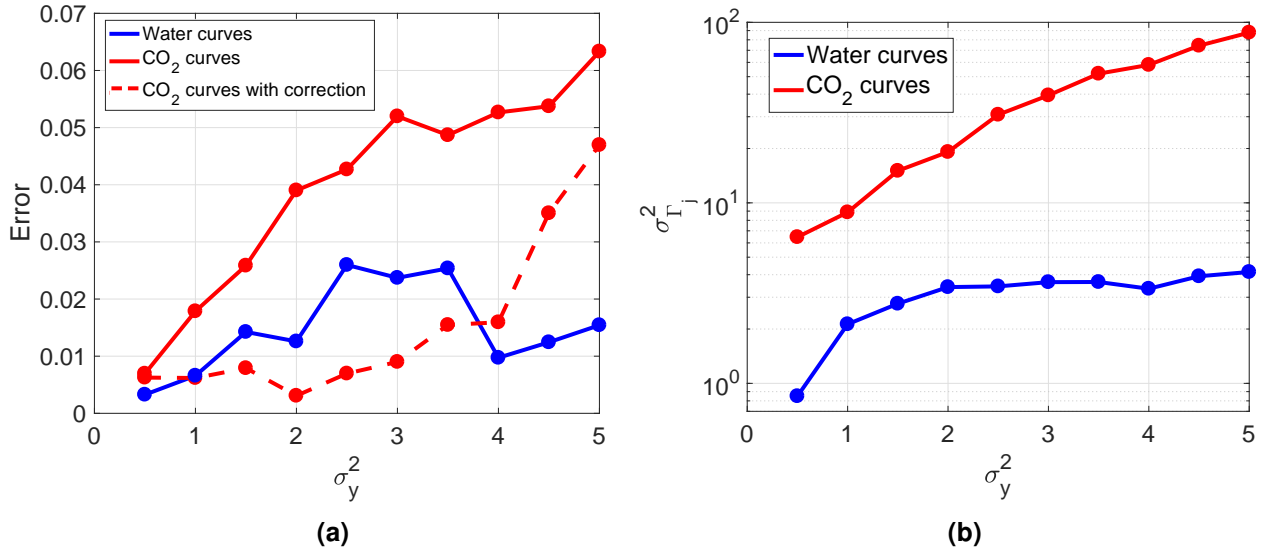


Figure 2: (a) Analytical method error and (b) variance of log phase permeability ($\sigma_{\Gamma_j}^2$) as a function of variance of log permeability (σ_y^2).

The water curves, on the other hand, show much smaller values of $\langle \sigma_{\Gamma_j}^2 \rangle$ which hardly increase with σ_y^2 and therefore the errors in Fig. 2a are smaller and do not increase consistently. We note that all errors in Fig. 2a are considered to be reasonable (under 0.1), even for σ_y^2 as large as 5 and the correction improves the error in all cases.

As discussed above, the analytical solution $k_{rCO_2}^{\text{eff}}(\tilde{P}_c, k)$ of Eq. (26) exhibits lower accuracy for large σ_y^2 and therefore a correction is derived. We consider a different power ω in Eq. (26) for each point on the $k_{rCO_2}^{\text{eff}}$ curve. The new power is defined by

$$\tilde{\omega}(\tilde{P}_c, m) = \omega \cdot \omega_c(\tilde{P}_c, m) \quad (27)$$

where ω_c is determined by matching the analytical and numerical solution for each point on the curve. The advantage of expressing corrections as a function of \tilde{P}_c and m is that these are existing parameters of the solution. The new solution for the CO₂ curves, incorporating the correction, is given by

$$k_{rj}^{\text{eff}} = \frac{1}{k_\omega} \left\{ \int_{-\infty}^{\infty} [K_j(\tilde{P}_c, k)]^{\tilde{\omega}(\tilde{P}_c, m)} p(y) dy \right\}^{1/\tilde{\omega}(\tilde{P}_c, m)}. \quad (28)$$

In Fig. 3 the correction $\omega_c(\tilde{P}_c)$ is presented for different values of σ_y^2 and m . It is evident that the correction remains approximately the same for k realizations of different σ_y^2 while varying m has a significant impact on $\omega_c(\tilde{P}_c)$. The structure of the curves appears to remain similar for changing

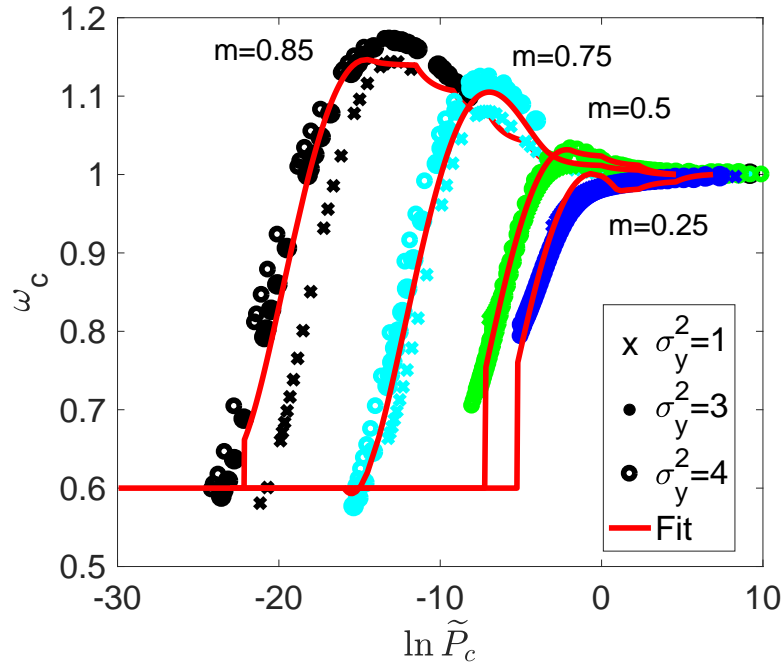


Figure 3: The correction to power law averaging (Eqs. (27),(28)) matching analytical and numerical CO₂ curves. VG J-function, varying m, σ_y^2 and $n_w = n_{CO_2} = 2$ are considered.

m so we proceed by fitting a polynomial function as follows

$$\omega_c(\tilde{P}_c, m) = \begin{cases} 0.6 & \ln \tilde{P}_c < L_{\text{lower}} \\ \hat{\omega}_c(\tilde{P}_c, m) & L_{\text{lower}} < \ln \tilde{P}_c < L_{\text{upper}} \\ [\hat{\omega}_c(e^{L_{\text{upper}}}, m) - 1] [\ln \tilde{P}_c - \ln \tilde{P}_c^{\text{max}}] / [L_{\text{upper}} - \ln \tilde{P}_c^{\text{max}}] + 1 & \ln \tilde{P}_c > L_{\text{upper}} \end{cases}, \quad (29)$$

where

$$\tilde{\omega}(\tilde{P}_c, m) = A_1 [\ln \tilde{P}_c - B_1(m)]^4 + A_2 [\ln \tilde{P}_c - B_1(m)]^3 + A_3 [\ln \tilde{P}_c - B_1(m)]^2 + A_4 \ln \tilde{P}_c + B_2(m),$$

$$\begin{aligned} B_1(m) &= C_1 m^3 + C_2 m^2 + C_3 m + C_4, & B_2(m) &= D_1 m^2 + D_2 m + D_3 - A_4 B_1(m), \\ A_1 &= 1.429 \cdot 10^{-4}, & A_2 &= 4.776 \cdot 10^{-3}, & A_3 &= 4.76 \cdot 10^{-2}, & A_4 &= 0.161, & C_1 &= -228.92, \\ C_2 &= 317.68, & C_3 &= -144.46, & C_4 &= 26.23, & D_1 &= 0.345, & D_2 &= -0.138, & D_3 &= 1.105, \\ L_{\text{upper}} &= -531.43 m^3 + 813.14 m^2 - 389.36 m + 55.82, & L_{\text{lower}} &= -58.26 m^2 - 35.89 m - 10.57, \end{aligned}$$

and \tilde{P}_c^{max} is the maximum chosen value for \tilde{P}_c .

We now test the approximate analytical solution given by Eqs. (15a,b), (22) and (27) - (29) for various values of m and σ_y^2 . The results are presented in Table 1, showing the maximum difference between analytical and numerical solutions. It can be seen that errors are fairly low with a largest error of 0.0628 and values under 0.03 for the vast majority of cases tested. We note that $m = 0.65, 0.8$ considered here were not used in the calibration of the correction (see

	Water curves (k_{rw}^{eff})				CO ₂ curves ($k_{rCO_2}^{eff}$)			
	$\sigma_y^2 = 1$	$\sigma_y^2 = 2$	$\sigma_y^2 = 3$	$\sigma_y^2 = 4$	$\sigma_y^2 = 1$	$\sigma_y^2 = 2$	$\sigma_y^2 = 3$	$\sigma_y^2 = 4$
$m = 0.85$	0.0119	0.0089	0.0102	0.0169	0.0264	0.0193	0.0381	0.0628
$m = 0.8$	0.0104	0.0168	0.0181	0.0111	0.0166	0.0161	0.0199	0.0293
$m = 0.75$	0.0066	0.0126	0.0237	0.0097	0.0062	0.0031	0.009	0.0159
$m = 0.65$	0.0108	0.0245	0.0360	0.0384	0.0068	0.0115	0.0169	0.0194
$m = 0.5$	0.0066	0.0204	0.0294	0.0283	0.0031	0.0058	0.0213	0.0618
$m = 0.25$	0.0034	0.0126	0.0216	0.0313	0.0017	0.0059	0.0056	0.01

Table 1: Error $\max \left| \left(k_{rj}^{eff}(\langle \tilde{S}_w \rangle) \right)_A - \left(k_{rj}^{eff}(\langle \tilde{S}_w \rangle) \right)_N \right|$ **for VG J-function with cases of different m and σ_y^2 ($n_w = n_{CO_2} = 2$).**

	Water curves (k_{rw}^{eff})			CO ₂ curves ($k_{CO_2g}^{eff}$)		
	$\sigma_y^2 = 1$	$\sigma_y^2 = 3$	$\sigma_y^2 = 4$	$\sigma_y^2 = 1$	$\sigma_y^2 = 3$	$\sigma_y^2 = 4$
$n_w = n_{CO_2} = 3$	0.0071	0.0097	0.0111	0.0106	0.0143	0.0175
$n_w = n_{CO_2} = 5$	0.007	0.0242	0.0103	0.0149	0.0299	0.0320

Table 2: Error $\max \left| \left(k_{rj}^{eff}(\langle \tilde{S}_w \rangle) \right)_A - \left(k_{rj}^{eff}(\langle \tilde{S}_w \rangle) \right)_N \right|$ **for VG J-function with cases of different n_w, n_{CO_2} and σ_y^2 ($m = 0.75$).**

Fig. 3) and this strengthens the reliability of its application. The current correction is intended for use only in the range $0.25 \geq m \leq 0.85$ and values outside this range are not presented here. Nevertheless, tests conducted indicate that for values of $m < 0.25$ the correction should still apply while for values of $m > 0.85$, error grows rapidly.

The analytical solution is tested further considering different values of the characteristic curve powers, n_w and n_{CO_2} in Eqs. (8a,b). Results are presented in Table 2, where maximum error is calculated as in the previous Table. It can be seen that increasing n_w and n_{CO_2} does not have a significant impact on the water curve error (see Table 1, $m = 0.75$ for comparison), while for the CO₂ curves a moderate increase of error is observed. We conclude from these results that the analytical solution remains accurate for larger values of n_w and n_g and an additional correction is not necessary.

Brooks-Corey capillary pressure

We now consider the BC J -function (Eq. (4)) in our formulation. The solution in this case is obtained by substituting Eqs. (17a,b) in Eq. (26). Results are presented in Fig. 4 for the parameters $n_w = n_{CO_2} = 2$ and $\lambda = 2$, used in previous literature for CO₂-brine flow modeling (Li, 2014; Rabinovich et al., 2015). It can be seen that the water curve analytical solution is in agreement with the numerical one, showing little to no error. The CO₂ curves, on the other hand, deviate substantially from the numerical solution, particularly for large σ_y^2 . A correction is necessary to accurately use the analytical solution for CO₂ curve modeling and this is discussed in the following. The corrected curves are plotted in Fig. 4 (dashed lines) and approximately match the numerical curves showing reasonable error.

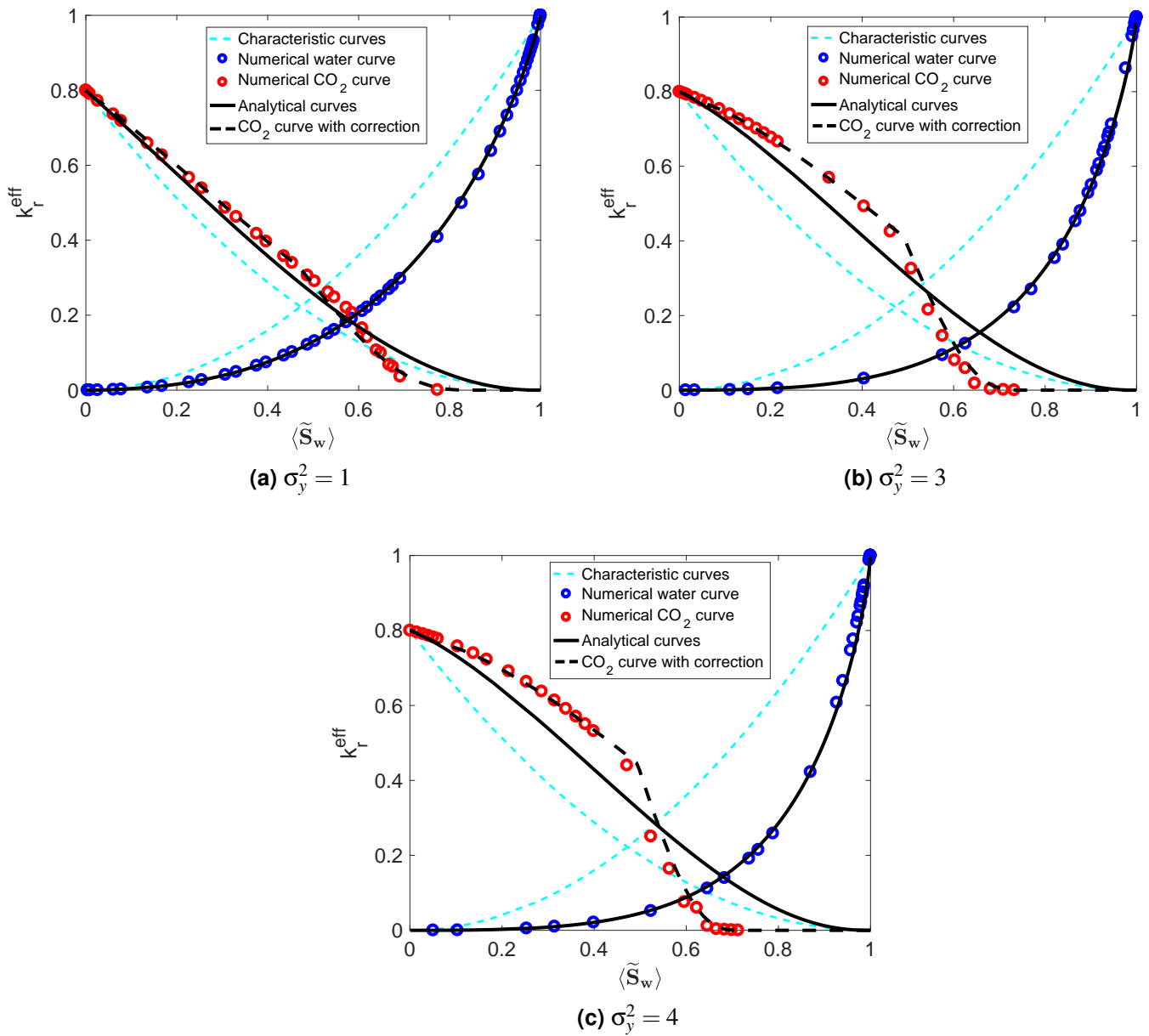


Figure 4: Core effective relative permeability as a function of water saturation in isotropic media with $l_x = l_y = l_z = 0.1$, $k_G = 100$ md, assuming BC J-function with $\lambda = 2$.

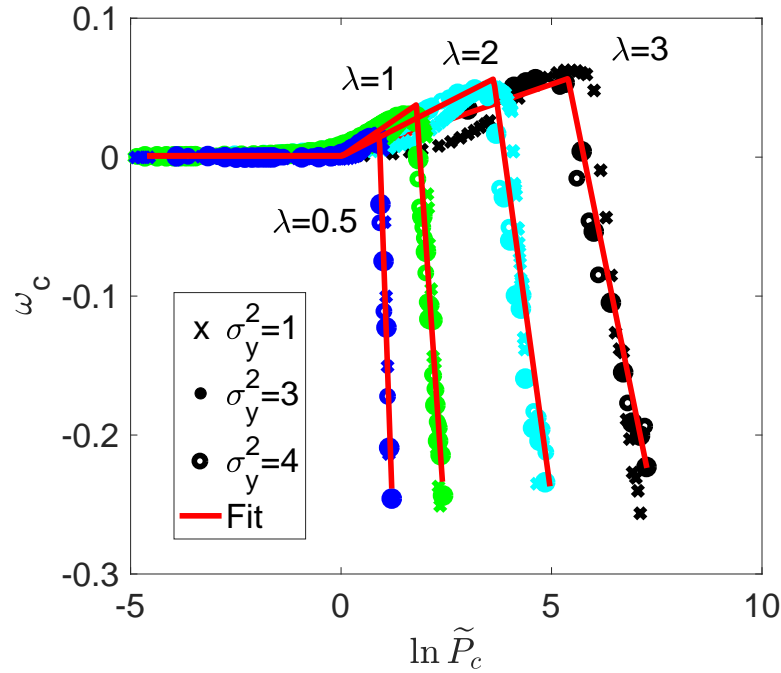


Figure 5: The correction to power law averaging (Eqs. (28), (30)) matching analytical and numerical CO₂ curves. BC J-function, varying λ , σ_y^2 and $n_w = n_{CO_2} = 2$ are considered.

The $k_{rCO_2}^{eff}$ structure apparent in Fig. 4 is different than in the VG case (see Fig. 1 for comparison) showing a sharp decrease at $\langle \tilde{S}_w \rangle \approx 0.4$ and reaching zero at smaller saturations. This is a result of capillary entry pressure, which by Eq. (17b) leads to many zero values in the K_{CO_2} field, reducing $k_{rCO_2}^{eff}$ at large $\langle \tilde{S}_w \rangle$. This effect is not captured by the analytical solution and therefore the correction is paramount.

The corrections for $k_{rCO_2}^{eff}$ is similar to that described for VG capillary pressure, i.e., considering different powers ω in Eq. (26). However, we find higher accuracy is achieved by defining the new power $\tilde{\omega}(\tilde{P}_c, \lambda)$ slightly different than in the previous case and as follows:

$$\tilde{\omega}(\tilde{P}_c, \lambda) = \omega + \omega_c(\tilde{P}_c, \lambda). \quad (30)$$

In Fig. 5 the correction $\omega_c(\tilde{P}_c)$ is presented for different values of σ_y^2 and λ . As in Fig. 3, the correction $\omega_c(\tilde{P}_c)$ shows little variation with σ_y^2 and a somewhat systematic change with λ . We fit the results with first degree polynomial (linear) functions. The result is given by

$$\omega_c(\tilde{P}_c, \lambda) = \begin{cases} 0 & \ln \tilde{P}_c \leq 0 \\ A'_1(\lambda) \left(0.0155 \ln \tilde{P}_c + 2.939 \cdot 10^{-4} \right) & 0 < \ln \tilde{P}_c < \tilde{P}_c^{intersect} \\ A'_2(\lambda) \left(0.905 - 0.235 \ln \tilde{P}_c \right) + A'_3(\lambda) & \ln \tilde{P}_c \geq \tilde{P}_c^{intersect} \end{cases}, \quad (31)$$

where

$$\begin{aligned}
 A'_1(\lambda) &= B'_1\lambda^3 + B'_2\lambda^2 + B'_3\lambda + B'_4 \\
 A'_2(\lambda) &= C'_1\lambda^3 + C'_2\lambda^2 + C'_3\lambda + C'_4, \quad A'_3(\lambda) = D'_1\lambda^5 + D'_2\lambda^4 + D'_3\lambda^3 + D'_4\lambda^2 + D'_5\lambda + D'_6, \\
 B'_1 &= 0.224, \quad B'_2 = -1.33, \quad B'_3 = 2.078, \quad B'_4 = 0.369, \\
 C'_1 &= -0.588, \quad C'_2 = 3.846, \quad C'_3 = -8.346, \quad C'_4 = 6.947 \\
 D'_1 &= 0.114, \quad D'_2 = -1.264, \quad D'_3 = 5.536, \quad D'_4 = -12.145, \quad D'_5 = 13.985, \quad D'_6 = -7.09
 \end{aligned}$$

and $\tilde{P}_c^{\text{intersect}}$ is the intersection of the two lines in Eq (31).

	Water curves (k_{rw}^{eff})				CO ₂ curves ($k_{rCO_2}^{\text{eff}}$)			
	$\sigma_y^2 = 1$	$\sigma_y^2 = 2$	$\sigma_y^2 = 3$	$\sigma_y^2 = 4$	$\sigma_y^2 = 1$	$\sigma_y^2 = 2$	$\sigma_y^2 = 3$	$\sigma_y^2 = 4$
$\lambda = 3$	0.0161	0.0127	0.0093	0.006	0.0749	0.0644	0.0283	0.0883
$\lambda = 2.5$	0.0155	0.0137	0.0095	0.0084	0.0826	0.0543	0.0169	0.095
$\lambda = 2$	0.0104	0.0123	0.0105	0.0083	0.0477	0.0293	0.0446	0.0881
$\lambda = 1.5$	0.007	0.0041	0.0053	0.0036	0.0507	0.0524	0.0442	0.0129
$\lambda = 1$	0.001	0.0073	0.0122	0.0136	0.0265	0.0209	0.0127	0.046
$\lambda = 0.75$	0.0036	0.0131	0.0168	0.0243	0.0112	0.0073	0.0295	0.0297
$\lambda = 0.5$	0.0063	0.0172	0.0305	0.0394	0.0083	0.0017	0.0055	0.0214

Table 3: Error $\max \left| \left(k_{rj}^{\text{eff}}(\langle \tilde{S}_w \rangle) \right)_A - \left(k_{rj}^{\text{eff}}(\langle \tilde{S}_w \rangle) \right)_N \right|$ **for BC J-function with cases of different λ and σ_y^2 ($n_w = n_{CO_2} = 2$).**

Table 3 presents results for the analytical solution given by Eqs. (17a,b), (22), (28), (30) and (31) for various values of λ and σ_y^2 . It can be seen that the error for the water curves is small in all cases with a maximum of 0.0394. For the CO₂ curves, error is larger with a maximum of 0.883. While all of the errors are within what we consider a tolerable range (< 0.1), the CO₂ curve errors are much larger than in the case of VG capillary pressure (see Table 1 for comparison). We note that $\lambda = 0.75, 1.5, 2.5$ considered here were not used in the calibration of the correction (see Fig. 5).

In Table 4, we consider different values of the characteristic curve powers, n_w and n_{CO_2} in Eqs. (8a,b). Analytical error in comparison with the numerical solution is presented, where maximum error is calculated as in the previous Table. It can be seen that increasing n_w does not have

	Water curves (k_{rw}^{eff})			CO ₂ curves ($k_{rCO_2}^{\text{eff}}$)		
	$\sigma_y^2 = 1$	$\sigma_y^2 = 3$	$\sigma_y^2 = 4$	$\sigma_y^2 = 1$	$\sigma_y^2 = 3$	$\sigma_y^2 = 4$
$n_w = n_{CO_2} = 3$	0.012	0.0099	0.0066	0.0212	0.0493	0.0915
$n_w = n_{CO_2} = 5$	0.0043	0.0033	0.003	0.0185	0.082	0.1287

Table 4: Error $\max \left| \left(k_{rj}^{\text{eff}}(\langle \tilde{S}_w \rangle) \right)_A - \left(k_{rj}^{\text{eff}}(\langle \tilde{S}_w \rangle) \right)_N \right|$ **for BC J-function with cases of different n_w, n_{CO_2} and σ_y^2 ($\lambda = 2$).**

a significant impact on the water curve error (see Table 3, $\lambda = 2$ for comparison). For the CO₂ curves at low variance ($\sigma_y^2 = 1$), the errors remain small, however, for larger variance ($\sigma_y^2 = 3, 4$) we begin to see a significant departure from the numerical solution.

Summary and conclusions

A method to correct core relative permeability for use in low flow rate CO₂ storage modeling is presented. Given the following core properties: capillary pressure, characteristic relative permeability (from high injection rate coreflooding experiments) and sub-core permeability geometric mean and log variance, we derive low flow rate effective relative permeability. The correction is given by an approximate semi-analytical solution assuming capillary limit conditions. The solution is based on power law averaging of the fine scale phase permeability field and is an exact solution in the case of one-dimensional (layered) permeability.

The semi-analytical solution is compared to a numerical one to test its accuracy. A wide range of cases are considered by varying the sub-core permeability field (σ_y^2), capillary pressure J -function type (VG or BC), J -function parameters (m, λ) and characteristic curve model (power in $k_{rj}(\tilde{S}_w) - n_w, n_{CO_2}$). It is shown that for all cases the analytical water curves approximately match the numerical solution. The CO₂ curves for a VG J -function type are accurate in cases of sufficiently small log permeability variance (σ_y^2). For larger σ_y^2 we derive a correction to the power ω in the averaging to improve accuracy. With the correction, it is shown that CO₂ curves are also estimated accurately for all cases. Considering a BC J -function type the analytical CO₂ curves show a large error due, in part, to the capillary entry pressure effect. A correction is presented, shown to reduce the error and reasonable agreement with the numerical solution is achieved in almost all cases. Only for the case of large powers in the characteristic curve model ($n_w = n_{CO_2} = 5$) with permeability of large σ_y^2 , errors exceeded the tolerable limit.

While the work presented here offers some insight on a general effective property problem, our main goal is to develop a method for practitioners to correct the core relative permeability measured in standard high rate coreflooding experiments. The analytical solution should allow for simple corrections without having to conduct additional low rate experiments or computationally demanding simulations. We have shown the method is robust, applicable to various types of cores and can be used in cases with significant capillary trapping (i.e., P_c curves with nonzero capillary entry pressure). Currently, the method is limited to drainage processes and an extension of the method for imbibition (in which hysteresis is important) should be considered in the future. Furthermore, it may be possible to extend the method to cores with permeability distributions other than the log-normal ones considered here.

Acknowledgements

This research was supported by Grant No. 2016182 from the United States-Israel Binational Science Foundation (BSF).

References

- H. Behzadi and V. Alvarado. Upscaling of upward CO₂ migration in 2D system. *Advances in Water Resources*, 46:46–54, 2012.
- A. Bielinski. *Numerical simulation of CO₂ sequestration in geological formations*. PhD thesis, University of Stuttgart, Stuttgart, Germany, 2007.
- R.H. Brooks and A.T. Corey. Properties of porous media affecting fluid flow. *Journal of the Irrigation and Drainage Division*, 92(2):61–90, 1966.
- H. Cao. *Development of Techniques for General Purpose Simulators*. PhD thesis, Stanford University, Stanford, CA, USA, 2002.
- A.T. Corey and C.H. Rathjens. Effect of stratification on relative permeability. *Journal of Petroleum Technology*, 8(12):69–71, 1956.
- C.V. Deutsch. Calculating effective absolute permeability in sandstone/shale sequences. *SPE Formation Evaluation*, 4:343–348, 1989.
- C.V. Deutsch and A.G. Journel. *GSLIB: Geostatistical Software Library and User's Guide*. Oxford University Press, New York, 1992.
- A.R. Freeze. A stochastic-conceptual analysis of one-dimensional groundwater flow in nonuniform homogeneous media. *Water Resources Research*, 11(5):725–741, 1975.
- A.G. Journel, C.V. Deutsch, and A.J. Desbarats. Power averaging for block effective permeability. In *SPE California Regional Meeting*. Society of Petroleum Engineers, 1986. SPE 15128.
- M. Krause, S.C. Krevor, and S.M. Benson. A procedure for the accurate determination of sub-core scale permeability distributions with error quantification. *Transport in porous media*, 98(3):565–588, 2013.
- M.H. Krause. Modeling and investigation of the influence of capillary heterogeneity on relative permeability. In *SPE Annual Technical Conference and Exhibition*. Society of Petroleum Engineers, San Antonio, Texas, SPE-160909-STU, 2012a.
- M.H. Krause. *Modeling and Investigation of the Influence of Capillary Heterogeneity on Multiphase Flow of CO₂ and Brine*. PhD thesis, Stanford University, 2012b.
- M.H. Krause and S.M. Benson. Accurate determination of characteristic relative permeability curves. *Advances in Water Resources*, 83:376–388, 2015.
- C-W. Kuo and S.M. Benson. Numerical and analytical study of effects of small scale heterogeneity on CO₂/brine multiphase flow system in horizontal corefloods. *Advances in Water Resources*, 79:1–17, 2015.
- C-W. Kuo, J.C. Perrin, and S.M. Benson. Effect of gravity, flow rate, and small scale heterogeneity on multiphase flow of CO₂ and brine. In *SPE Western Regional Meeting*. Society of Petroleum Engineers, Anaheim, CA, SPE 132607, 2010.
- M.C. Leverett. Capillary behavior in porous solids. *Transactions of the AIME*, 142:152–169, 1941.
- B. Li. *Modeling geological CO₂ sequestration: Translations across spatial scales and advancements in nonlinear Newton solver*. PhD thesis, Stanford University, 2014.
- B. Li and S.M. Benson. Influence of small-scale heterogeneity on upward CO₂ plume migration in storage aquifers. *Advances in Water Resources*, 83:389–404, 2015.
- B. Li, H.A. Tchelepi, and S.M. Benson. Influence of capillary-pressure models on CO₂ solubility trapping.

- Advances in Water Resources*, 62:488–498, 2013.
- A. Lohne, G.A. Virnovsky, and L.J. Durlofsky. Two-stage upscaling of two-phase flow: From core to simulation scale. *SPE Journal*, 11(3):304–316, 2006.
- E. Mouche, M. Hayek, and C. Mügler. Upscaling of CO₂ vertical migration through a periodic layered porous medium: The capillary-free and capillary-dominant cases. *Advances in Water Resources*, 33(9):1164–1175, 2010.
- I. Neuweiler, A. Papafotiou, H. Class, and R. Helmig. Estimation of effective parameters for a two-phase flow problem in non-gaussian heterogeneous porous media. *Journal of contaminant hydrology*, 120:141–156, 2011.
- Z.S. Omoregle. Factors affecting the equivalency of different capillary pressure measurement techniques. *SPE formation evaluation*, 3(1):146–155, 1988.
- J.C. Perrin and S.M. Benson. An experimental study on the influence of sub-core scale heterogeneities on CO₂ distribution in reservoir rocks. *Transport in Porous Media*, 82(1):93–109, 2010.
- J.C. Perrin, M. Krause, C.W. Kuo, L. Miljkovic, E. Charoba, and S.M. Benson. Core-scale experimental study of relative permeability properties of CO₂ and brine in reservoir rocks. *Energy Procedia*, 1(1):3515–3522, 2009.
- G.E. Pickup and K.S. Sorbie. Scaleup of two-phase flow in porous media using phase permeability tensors. *SPE Journal*, 1(4):369–382, 1996.
- R. Pini and S.M. Benson. Characterization and scaling of mesoscale heterogeneities in sandstones. *Geophysical Research Letters*, 40(15):3903–3908, 2013.
- R. Pini, S.C.M Krevor, and S.M Benson. Capillary pressure and heterogeneity for the CO₂/water system in sandstone rocks at reservoir conditions. *Advances in Water Resources*, 38:48–59, 2012.
- A. Rabinovich. Estimation of sub-core permeability statistical properties from coreflooding data. *Advances in Water Resources*, DOI: 10.1016/j.advwatres.2017.07.012, In Press, 2017.
- A. Rabinovich, K. Itthisawatpan, and L.J. Durlofsky. Upscaling of CO₂ injection into brine with capillary heterogeneity effects. *Journal of Petroleum Science and Engineering*, 134:60–75, 2015.
- A. Rabinovich, B. Li, and L.J. Durlofsky. Analytical approximations for effective relative permeability in the capillary limit. *Water Resources Research*, 52(10):7645–7667, 2016.
- N. Remy, A. Boucher, and J. Wu. *Applied Geostatistics with SGeMS: A User's Guide*. Cambridge University Press, Cambridge, UK, 2009.
- J.G. Richardson, J.K. Kerver, J.A. Hafford, and J.S. Osoba. Laboratory determination of relative permeability. *Journal of Petroleum Technology*, 4(8):187–196, 1952.
- P.S. Ringrose, K.S. Sorbie, P.W.M Corbett, and J.L. Jensen. Immiscible flow behaviour in laminated and cross-bedded sandstones. *Journal of Petroleum Science and Engineering*, 9(2):103–124, 1993.
- M.T. van Genuchten. A closed-form equation for predicting the hydraulic conductivity of unsaturated soils. *Soil science society of America Journal*, 44(5):892–898, 1980.
- G.A. Virnovsky, H.A. Friis, and A. Lohne. A steady-state upscaling approach for immiscible two-phase flow. *Transport in Porous Media*, 54(2):167–192, 2004.
- N. Wei, M. Gill, D. Crandall, D. McIntyre, Y. Wang, K. Bruner, X. Li, and G. Bromhal. CO₂ flooding properties of liujiagou sandstone: influence of sub-core scale structure heterogeneity. *Greenhouse Gases: Science and Technology*, 4(3):400–418, 2014.